

## **Deformation near the Coyote Creek fault, Imperial County, California: tectonic or groundwater-related?**

Robert J. Mellors and Alex Boisvert<sup>1</sup>  
Dept of Geological Sciences, San Diego State University  
San Diego CA 92122

<sup>1</sup> Now at Schlumberger, Bakersfield, CA

**Abstract.** Interferometric synthetic aperture radar (InSAR) measurements show a consistent, 40-km<sup>2</sup> wedge-shaped area of deformation partially bounded by a branch of the Coyote Creek fault (a southern extension of the San Jacinto fault) in Imperial County, California west of the Salton Sea. The deformation is centered at 33.1 N latitude, 116.0 W longitude. 11 ERS-1 and ERS-2 (descending) interferograms falling within 1992 to 2000 are analyzed. A roughly 8 mm (maximum) line-of-sight range change (away) per year is observed. The western edge of the deformation is partially bounded by a fault segment that ruptured in the 1968  $M_w$  6.5 Borrego Mountain earthquake and also showed triggered slip after the 1987 Superstition Hills earthquakes. The southern edge of the deformation also coincides with a mapped fault. The area of deformation is centered on a farming area that pumps groundwater from 5 wells on the property. Between 1995 and 1997 the average rate of pumping was approximately  $5.8 \times 10^6$  m<sup>3</sup> per year. The area of highest change appears to be centered on location of the wells and away from the boundaries. The aquifer is at a depth of roughly 100 to 200 m and consists of sands with interbedded clays. Clays comprise approximately 20% of the well log. It appears that the most likely explanation is subsidence due to groundwater withdrawal and compaction of fine-grained layers. Preliminary calculations suggest that these effects can easily explain both the magnitude and geometry of subsidence. We speculate that groundwater effects may have enhanced some of the earthquake-related features previously reported.

## **Introduction.**

One of the most seismically active faults in Southern California is the San Jacinto fault, which lies west of the San Andreas. The San Jacinto fault has generated earthquakes with magnitudes greater than 6 four times in the past 100 years alone (Figure 1). The most recent event was the 1968  $M_w$  6.5 Borrego Mountain earthquake [Allen *et al.*, 1968]. The region is more populated now, and a repeat event would almost certainly cause considerable damage.

Recently, Vincent [1998; 2000] observed an area of deformation along the Coyote Creek segment of the southern San Jacinto using interferometric synthetic aperture radar (InSAR). As the Coyote Creek segment ruptured in 1968 during the Borrego Mountain earthquake and showed triggered slip in 1987 after the Superstition Hills earthquake, aseismic tectonic slip appears to be one obvious possibility [Vincent, 2000]. This is significant, as it would indicate that some of the tectonic stress is being released and therefore likely reduce the seismic hazard. In this paper we undertake a closer examination of the area using a different and larger SAR dataset as well as additional local geologic and hydrologic data. The deformation is confirmed to lie very near the mapped Coyote Creek fault and is bounded by a fault segment that ruptured in the 1968 event. However, the area of deformation is centered on a farm that pumps considerable amounts of groundwater and subsidence related to aquifer draw down may explain the observed features (rather than tectonic slip).

This is important for several reasons. First, it suggests that tectonic stress is not being released and consequently the seismic hazard is not reduced. Second, it reinforces the concept [Bawden *et al.*, 2001; Watson *et al.*, 2001; Massonet *et al.*, 1997] that attempts to estimate hazard using ground deformation even near faults with recent ruptures must consider aquifer-related deformation. As a considerable effort has been made to measure ground deformation using space geodetic methods such as GPS and INSAR in southern California with the hope of determining the regional tectonic signal it is important to characterize all other sources of movement and especially sources located near major faults. Finally, non-tectonic movements along the Coyote Creek fault may add additional error to some of the paleoseismic slip estimates.

*Tectonic and geologic setting.* The difference in plate motion between North America and the Pacific Plate is accommodated by three major faults in Southern California: the San Andreas, the San Jacinto, and the Elsinore (Figure 1). Between the San Andreas and the San Jacinto is the Salton trough, a Miocene age rift valley. As the southern San Jacinto fault zone enters the Salton Trough from the northwest, it splits into several major fault strands and a number of cross-faults [Sharp, 1972; Rockwell *et al.*, 1990; Petersen *et al.*, 1991]. The southernmost branch is the Coyote Creek segment, which has been the subject of numerous geodetic, seismological, and paleoseismological investigations [Magistrale, 2001; Altangeral, 2001; Sanders *et al.*, 1986] as well as extensive investigations after the 1968 and 1987 earthquakes [Burford, 1972; Clark, 1972a; Clark, 1972b, Clark *et al.*, 1972; Hudnut and Clark, 1989; Hudnut *et al.*, 1989].

The area of deformation occurs in a mostly flat area of Holocene sediments overlaying Pliocene-Pleistocene sediments [Clark *et al.*, 1972] near the western edge of the Salton Trough. The Holocene sediments include Lake Coahuilla deposits, a precursor to the Salton Sea [Jennings, 1967]. The depth to basement is estimated at 3 km [Burford, 1972].

Seismicity is pronounced and occurs on both the major faults and the cross-faults [Petersen *et al.*, 1991; Magistrale, 2001]. The 1968 Borrego Mountain earthquake occurred along the Coyote Creek fault and produced a 31 km long rupture with up to 380 mm of mostly right-lateral motion [Clark, 1972a]. A distinguishing feature of the Borrego Mountain earthquake was the amount of post-seismic slip that occurred on the Coyote Creek as well as triggered slip on nearby faults. The 1987 M 6.2 Elmore Ranch/M 6.6 Superstition Hills events (which occurred within 12 hours of each other) were roughly 20 km to the south and ruptured both the northeast-southeast Superstition Hills fault and a cross fault.

Recent GPS data [SCEC, 2001] show an east-west gradient in the plate motion vectors west of the San Andreas and suggests considerable strain in the region (Figure 1). The slip rate along the southern San Jacinto (Lower Borrego Valley) is estimated to be between 1.4 and 5.0 mm per year based on paleoseismic data [Peterson and Wesnousky, 1994]. Slip rates along the Coyote Creek segment are more uncertain but are likely to be

approximately 3 mm per year [Clark *et al.*, 1972]. Recent paleoseismic work on the Coyote Creek segment very near the area of deformation shows a history of repeated ruptures but no evidence of surface creep along the main fault [Altangerel, 2001].

### **Data and method.**

We use C band (5.66 cm) data from the ERS-1 and ERS-2 satellites (Figure 1 and Table 1) to generate a number of interferometric phase measurements [e.g. Burgman *et al.*, 2000]. The data were acquired through the WINSAR program. SAR processing was performed using a range-Doppler algorithm as part of the SIOSAR [Price, 1997] package. Standard INSAR processing was conducted using precise orbits [Scharoo and Visser, 1998] and a combination of a 90 m USGS DEM and a tandem pair to eliminate topography effects. 11 pairs from track 127, frame 2943 (descending) were processed. For these data, the look angle is 23° off vertical and points S 77° E. Only the pairs with relatively short baselines and longer temporal span were used to measure deformation (pairs with longer baselines and short time span were used to refine the elevation model). Several showed severe atmospheric effects. The data shown here were selected for the highest signal and had a best-fit plane removed to reduce long-wavelength effects, which are probably due to orbit errors.

Correlation is fairly high, with some pixels retaining correlation for as long as 5 years. Most of the rapid decorrelation is due to vegetation in farm fields and along washes. Some decorrelation is due to sand movement from wind or off-road vehicles [Boisvert, 2001]. Apparent atmospheric noise, which appears as areas of varying phase change with amplitudes on the order of one fringe, appears on several images.

### **Results.**

*Pattern of deformation.* The results clearly show an irregular area with movement away along radar line-of-sight on several pairs (Figures 2 and 3). The deformation is roughly wedge-shaped, with the western and south margins having generally sharp boundaries while the north and east edges shows a slow decrease of deformation in a radial pattern. The amount of change is greatest near the center of the wedge, which is partially masked by areas of high decorrelation on all images. The decorrelation

coincides with the farm fields as observed by optical images and verified by ground truth field visits. The deformation appears on several pairs of INSAR scenes, including pairs with completely independent scenes, indicating that it is not due to atmospheric effects. It also appears on a pair with a perpendicular baseline of 5 m that was processed without an elevation correction showing that errors in the topographic model used for the correction are not an explanation. As the area is very flat errors in topography seem unlikely. The sense of motion is the same (away) on all pairs. The two scenes (A and C in Figure 2) with lowest noise were normalized by time and then stacked to determine an approximate yearly subsidence rate of 8 mm in the peak areas (Figure 4). As only the line-of-sight motion can be measured with this data set, determining vertical or horizontal components is not possible. However, this would correspond to roughly 10 mm of vertical movement but would require much more purely horizontal movement.

Approximate subsidence estimates were made along cross-section C (Figure 2) by filtering the data with coherence greater than 2 and then estimating the subsidence from the northeast and from the southwest to the data gap at the center. These two estimates were then averaged to yield the values in Table 1. Note that these values are smaller than the peak estimate derived from Figure 4. Approximate errors were estimated by determining the standard deviation of the data shown in Figure 2 after removing the expected subsidence (using the yearly estimate shown in Figure 4).

*Relationship to surface rupture and known faults.* The 1968 earthquake showed three major surface breaks: the north, central and south breaks [Clark, 1972a]. Slip was generally expressed as right-lateral en echelon breaks with a maximum shift of 38 cm on the north break. One curious feature was the occurrence of numerous collapse fissures associated with the surface rupture (Clark, 1972b). Most movement took place along the Coyote Creek fault which lies about 1-2 km to the west of the western edge of the deformation. However, one isolated segment of surface rupture along the middle break occurred slightly to the east and just south of the Ocotillo Badlands and showed approximately 20-80 mm of likely co-seismic right-lateral movement. The width of the fracture zone was roughly 3 m. Considerable additional movement occurred as post-

seismic slip as well on this segment (Clark, 1972a). It is this segment that matches the western edge of the deformation.

Post-seismic slip was along the central break was dramatic with as much as 31 cm of right-lateral horizontal movement (as compared to 13 cm during the initial break). Some vertical slip (down on the northeast) was also observed. The slip decreased logarithmically with time. In contrast, the northern break showed very little post-seismic slip although the total slip on the segments was similar. No large aftershocks were associated with this creep so it is effectively aseismic (although following a large event). This behavior was interpreted as slip propagating up through the thick sedimentary cover with time [Burford, 1972]. In 1987, this segment again showed slip, this time apparently triggered by the Elmore Ranch/Superstition Hills events where up to 8 mm of right-lateral slip was observed [Hudnut and Clark, 1989].

The south edge of the deformation also appears as a fairly sharp boundary on several (but not all) interferograms. This suggests that it is also due to a fault. The orientation is similar to other cross faults in the area and it may match with a fault zone noted by Hudnut *et al.*, [1989] (the “Extra” fault).

The high rates of slip observed both seismically and aseismically in the area provide one possible explanation for the observed deformation. Two major inconsistencies must be explained. First, the sense of motion of the deformation is not consistent with the expected right lateral slip along the Coyote Creek. Second, the amount of range change is at a maximum away from the fault for most of the interferograms. Movement along a conjugate fault [Vincent, 2000] might allow for the direction of motion, especially if the movement had a substantial proportion of vertical motion. The apparent increase away from the fault might be explained by coincidental atmospheric errors on two or more scenes. Consequently, it is impossible to rule out a tectonic explanation; however an alternate explanation, and in our opinion, a simpler explanation, is available.

*Ground water.* As noted above, the area of deformation is centered on a roughly 200-hectare farm located about 3 miles east of the San Diego/Imperial County border on Highway 78. This farm has six wells, five of which extract substantial amounts of water

for irrigation purposes (Table 2 and Figure 5). Ground water withdrawal often produces signals that are well-recorded by InSAR [Massonet *et al.*, 1997; Amelung *et al.*, 1999; Galloway *et al.*, 1998; Bawden *et al.*, 2001].

Well data, water extraction information for recent years, and an unpublished 1970 hydrologic report were made available by the owners of the farm. Aerial photos indicate that the farm existed in 1968 and the groundwater report indicates that some extraction was going on at that time. The available geologic data consists of information on the perforated intervals of these wells, the estimated permeable strata within this interval, and a description of the lithology. Unfortunately, information on the water level over time was not available for the period covered by the InSAR data. The average percentage of impermeable strata within the perforated intervals is 20 percent. Well logs indicate these impermeable intervals are consisted mostly of silts and clays while the aquifers consist of fine to coarse sands, with isolated intervals of gravels.

Subsidence due to groundwater withdrawal depends largely on the lithology of the subsurface. Water extracted from an aquifer composed solely of sand and gravel can often be recharged naturally or anthropogenically, with no appreciable permanent subsidence. However, aquifer systems with interbedded or adjacent impermeable beds may suffer permanent damage. As water is extracted from the aquifer, the decline in head level causes a reduction in pore pressure in the impermeable layers. Water held in the layer can then be released, causing compaction of the beds. This reduction in bed thickness causes irreversible subsidence. Although aquifers can compact, it has been found that subsidence is controlled substantially more by the compaction of aquicludes than aquifers in systems containing both [Galloway *et al.*, 1998].

Natural recharge to the aquifer is believed to be negligible as the desert receives an average of three to five inches of rainfall per year and most water that enters the soil is captured by plant life before it reaches depths capable of producing any natural recharge. In addition, several clay layers separate the aquifer from the surface. The aquifer is estimated to hold  $7.1 \times 10^9$  m<sup>3</sup> of water [Koebig and Koebig, unpublished report, 1970].

The volume of water removed is approximately  $5.8 \times 10^6$  m<sup>3</sup> per year. Assuming approximately 8 mm of subsidence per year, the total volume loss is approximately 6% of the water volume. Values for other regions have ranged as high as 30% of the water

volume, so these numbers are well within other observed values. These numbers are very approximate, as water will flow into the aquifer from outside the region of observed subsidence. Typically, draw down (and hence subsidence) is most pronounced near the wells and decreases radially away. This is observed in the case as the highest subsidence occurs at the edges of the decorrelated region near the location of the wells and decreases slowly to the north and east.

Pumping rates are not constant during the year (Figure 5). This should cause changes in rate of subsidence and in principle, severe reduction of pumping (as occurred in the later part of 1997) might result in uplift, as the head level at the wells should raise and increase pore pressures. The uplift rate would depend on the aquifer geometry and lithology and would likely be much smaller (in absolute value) than the subsidence rates. As the time periods of known reduced pumping (3 months) were short the amount of uplift, if any, is likely to be small (on the order of 1 mm) and consequently unlikely to be observed in this data set. No clear evidence of uplift is observed in the dataset. A clear signal would provide strong evidence for a groundwater-related signal.

The linear edge at the location of the faults to the west and south suggest that the faults are sealing the aquifer, which prevents water flowing in and increases the amount of draw down (Figure 6). The confined nature of the aquifer also leads to a much larger area of draw down than for an unconfined aquifer. The southern boundary is also slightly more pronounced and this may imply that a fault borders the aquifer to the south and that this fault has been active since deposition of the aquifer.

The hydrological report as well as other work suggests that faults act as barriers of groundwater flow in the area [Koebig and Koebig, unpublished report, 1970; Moyle, 1982; Clark, 1972]. Fault sealing evidence is based on water-level contours that show that the ground water flows parallel to faults in most places. Three major explanations for this are: reduced permeability in the rupture zones caused by fault gouge, offset of beds with variable permeability on either sides of the fault, and filling of cracks related to fault movement with impermeable sediment. Although the third mechanism has not been documented in this region, it has been noted in similar desert environments [Moyle, 1982].

## **Discussion and conclusions.**

In this case it appears that the observed InSAR signal is most likely due to aquifer lowering as the sense of motion, geometry, and magnitude of the deformation matches that expected from the known groundwater production and subsurface geology. The sharp boundaries near the faults can be explained by fault sealing of the aquifer and the more gradual boundary at the northeast matched the expected head levels. Finally, the localization of the highest rates of subsidence near the location of the wells rather than the faults (as would be expected for tectonic motion) is strong evidence in favor of subsidence related to groundwater withdrawal. It is possible that there is some tectonic component, but it is not required.

It is not clear (due to the limits of resolution) whether the vertical subsidence is taking place along the fault itself (as vertical slip). The motion of a few mm per year would be difficult to identify visually. It is interesting to speculate what effect a large earthquake (either on this fault or a nearby fault) might have on a shallow, overdrawn aquifer bounded by a fault. Strong shaking might cause further compaction of the drained layers and differential subsidence across the fault. Subsidence related to the aquifer might also explain the collapse fissures noted by Clark (1972*b*). Alternatively, seismic waves should increase pore pressures temporarily. It is striking that the edge of the deformation matches closely with peak areas of post-seismic slip and later triggered slip. Perhaps movement related to the subsidence has weakened the fault at shallow depths.

The results of this study also reinforces the idea that aquifer-related signals are highly important even in areas of known tectonic motion. However, it is also clear that the signal matches the expected aquifer signal and therefore might be subtracted from the measured signal after modeling [Galloway *et al.*, 2001]. Finally, a practical use is to map the actual aquifer draw down at high spatial detail without drilling test wells, which would be useful in estimating the remaining water reserves.

*Acknowledgements.* This work was conducted with support from NASA grant NAG5-8560 to R. Mellors. Synthetic aperture radar data was provided by the European Space Agency through their North American distributors Eurimage and SpotImage and purchased by the WInSAR consortium with funding from NASA, NSF and USGS. Figures were constructed using GMT software (Wessel and Smith, 1991). The work greatly benefited from discussions with D. Ragona, P. Vincent, G. Bawden, and K. Hudnut.

## References.

Allen, C. R., A. Grantz, J. N. Brune, M. M. Clark, R. V. Sharp, T. G. Theodore, E. W. Wolfe, and M. Wyss, The Borrego Mountain, California, earthquake of 9 April, 1968: A preliminary report, *Bull. Seismo. Soc. Amer.*, **58**, (3), 1183-1186, 1968.

Altangerel, O., 2001, "Three-Dimensional Paleoseismic Investigation of the South Break of the Coyote Creek Fault, Southern California," M.S. Thesis, San Diego State University, 2001.

Amelung, F., D. L. Galloway, J. W. Bell, H. A. Zebker, R. J. Laczniaik, Sensing the ups and downs of Las Vegas: InSAR reveals structural control of land subsidence and aquifer-system deformation, *Geology*, **27**, p. 483-486, 1999.

Bawden, G. W., W. Thatcher, R. S. Stein, K W. Hudnut, and G. Peltzer, Tectonic contraction across Los Angeles after removal of groundwater pumping effects, *Nature*, **412**, 812-815, 2001.

Boisvert, A., Synthetic aperture radar coherence and interferometric study of San Diego County, California, MS thesis, San Diego State University, 2001.

Burford, R. O., Continued slip on the Coyote Creek Fault after the Borrego Mountain earthquakes, The Borrego Mountain earthquake of April 9, 1968, U.S.G.S. professional paper, P 0787, pp. 105-111, 1972.

Burgmann, R., P.A. Rosen, and E.J. Fielding, Synthetic aperture radar interferometry to measure Earth's surface topography and its deformation: *Ann. Revs. Earth Planet. Sci.*, **28**, 169-209, 2000.

Clark, M. M., Surface rupture along the Coyote Creek fault: in The Borrego Mountain Earthquake of April 9, 1968: U. S. Geological Survey Professional Paper 787, pp. 55-86, 1972.

Clark, M. M., Collapse fissures along the Coyote Creek fault: in The Borrego Mountain Earthquake of April 9, 1968: U. S. Geological Survey Professional Paper 787, pp. 190-207, 1972.

Clark, M. M., A. Grantz, and M. Rubin, Holocene activity of the Coyote Creek segment as recorded in sediments of Lake Cahuilla: in The Borrego Mountain Earthquake of April 9, 1968: U. S. Geological Survey Professional Paper 787, pp. 112-130, 1972.

Galloway, D.L., K.W. Hudnut, S.E. Ingebritsen, S.P. Phillips, G. Peltzer, F. Rogez, and P.A. Rosen, Detection of aquifer system compaction and land subsidence using interferometric synthetic aperture radar, Antelope Valley, Mojave Desert, California, *Water Resources Research*, **34**, 2573-2585, 1998.

Hudnut, K. W. and M. M. Clark, New slip along parts of the 1968 Coyote Creek fault rupture, California, *Bull. Seismo. Soc. Amer.*, **79**, 451-465, 1989.

Hudnut, K. W., L. Seeber, and J. Pacheco, Cross-fault triggering in the November 1987 Superstition Hills earthquake sequence, southern California, *Gephys. Res. Let.*, **16**, (2), 199-202, 1989.

Jennings, C. W., Geologic map of California, Salton Sea sheet, scale 1:250,000, Calif. Div. Mines and Geology, Sacramento, 1967.

Magistrale, H., The Relation of the Southern San Jacinto Fault Zone to the Imperial and Cerro Prieto Faults, submitted to the Geological Society of America special volume in honor of Perry Ehlig, 2001.

Massonnet, D., Holzer, T., and Vadon, H., Land subsidence caused by the East Mesa geothermal field, California, observed using SAR interferometry: *Geophys. Res. Let.*, **24**, 901-904, 1997.

Moyle, W. R., Jr, Water resources of Borrego Valley and Vicinity, California Phase 1-Definition of Geology and Hydrologic Characteristics of Basin: U.S. Geological Survey, Open File Report 82-855, 1982.

Petersen, M. D., L. Seeber, L. R. Sykes, J. L. Nabelek, J. G. Armbruster, J. Pacheco, and K. W. Hudnut, Seismicity and fault interaction, southern San Jacinto fault zone and adjacent faults, southern California: Implications for seismic hazard, *Tectonics*, **10**, 1187-1203, 1991.

Petersen, M. D. and S. G. Wesnousky, Fault slip rates and earthquake histories for active faults in southern California: *Bull. Seismo. Soc. Amer.*, **84**, (5), 1,608-1,649, 1994.

Pollard, W. J. and Rockwell, T. K., 1995, Late Holocene slip rate for the Coyote Creek fault, Imperial County, California (abstract): Geological Society of America, Abstracts with programs, **27**, 5, p. 72, 1995.

Price, E., Coseismic and postseismic deformations associated with the 1992 Landers, California, earthquake measured by synthetic aperture radar interferometry, Ph.D thesis, University of California, San Diego, 1997.

Sanders, C., H. Magistrale, and H. Kanomori, Rupture patterns and preshocks of large earthquakes in the southern San Jacinto fault zone, *Bull. of the Seismo. Soc. Amer.*, **76**, (5), 1187-1206, 1986.

Scharroo, R. and P. Visser, Precise orbit determination and gravity field improvements for the ERS satellites, *J. Geophys. Res.*, **102**, 8113-8127, 1998.

Southern California Earthquake Data Center (SCEDC), Retrieved on October 1, 2001, from SBDC Southern California plate motion site: <http://www.scecdc.scec.org>, 2001.

Sharp, R. V., Tectonic setting of the Salton Trough: in The Borrego Mountain Earthquake of April 9, 1968: U. S. Geological Survey Professional Paper 787, pp. 3-15, 1972.

Rockwell, T. K., Loughman, C., and Merifield, P., Late Quaternary rate of slip along the San Jacinto fault zone near Anza, southern California: *J. Geophys. Res.*, **95**, 8593-8605, 1990.

Rockwell, T. R. Blom, R. Crippen, R. Klinger, A. Stinson, and A. Thomas, Recognition, extension, and significance of northeast trending faults between between the Elsinore and San Jacinto fault zones using combined SPOT and Landsat imagery, Friends of the Pleistocene Fieldtrip guidebook – Western Salton Trough soils and Neotectonics, 105-125, 1990.

Vincent, P. Aseismic slip events along the southern San Andreas fault system captured by radar interferometry, Proceedings of the 3<sup>rd</sup> conference on tectonic problems of the San Andreas fault system, September 6-8, Stanford University, 2000.

Vincent, P., Application of SAR interferometry to low-rate crustal deformation fields, Univ. of Colorado, Boulder, Ph.D thesis, p. 218, 1998.

Wessel, P. and W. H. F. Smith, Free software helps map and display data, *Eos Trans. AGU*, 72(441), 445-446, 1991

Watson, K. M., Yehuda Bock, David T. Sandwell, 2001, Satellite interferometric observation of displacements associated with seasonal ground water in the Los Angeles Basin, submitted to *J. Geophys. Res.*, February 15, 2001.

**Figure 1.** Regional shaded topography map showing area covered by the InSAR scene (track 127 scene 2943) and a small box (red) showing the area of interest. Faults (red) and historical earthquakes are also marked (large red and white circles, with white denoting poorly constrained epicenters). Small yellow dots indicate well-located seismicity between 1985 and 2000 [Magistrale, 2001]. Arrows show average plate motion vector with respect to North America as measured by GPS [SCECDC]. Only a subset of the available vectors is shown. The largest arrows represent approximately 40 mm per year of movement.

**Figure 2.** (A). Line-of-sight range change map for May 23, 1995 to Sep 26 – 1996. Pixels with coherence less than 0.2 are grayed out. The scarp of the 1968 Borrego Mountain rupture is shown in black. Water wells are shown as circles with dots at center. Units are mm. (B). Coherence image of the same pair as in A. Dark is low coherence, white is high. Locations of water wells are shown as red dots. (C) Inteferogram for May 23, 1995 to Jan 8, 1998. (D) 1996 to 2000. The threshold is 0.15 for the pixel coherence and a different scale is used. Discontinuities indicate that unwrapping errors are present in this image. Data is copyright of the European Space Authority (ESA).

**Figure 3.** Cross-sections showing line-of-sight range change in mm and topography (line) corresponding to the lines drawn in image A on Figure 2. Only pixels with coherence  $> 0.2$  are shown. Cross-sections go from southwest (right) to northeast (left).

**Figure 4.** Map of area with contours showing average line-of-sight subsidence per year (mm) generated from a smoothed average of the two pairs May 1995-Sep 1996 and May 1995 >. The signal has been interpolated across low coherence pixels. Circles denote water wells with dots at the center.

**Figure 5.** Graph of volume of water pumped per month (dots) at bottom and estimated subsidence measured from InSAR pairs. The estimated subsidence is from a filtered version of cross-section C from Figure 3. Letters correspond to images shown in Figure 2. Error bars are based on the standard deviation of the points in Figure 2 after removal of the average subsidence based on a stack of normalized data from all pairs.

**Figure 6.** Cartoon schematic of the expected head level in a confined aquifer unbounded on one side and with a vertical boundary on the other. The expected subsidence would be proportional to the head level and therefore explain the asymmetrical cross-section observed in Figure 3.

**Table 1.** SAR scenes and time spanned. Parameters and estimated range change for the images shown in this paper. These are a subset of the larger set processed. Errors on the range change represent 1 standard deviation of the points in Figure 2 after removal of the average subsidence based on a stack of normalized data from all pairs.

**Table 2.** Gross perforated intervals, estimated permeable strata within the interval, and percentage of impermeable strata within each interval for the wells. The impermeable layers are likely more susceptible to compression leading to subsidence after fluid withdrawal.

**Table 1.** SAR interferogram pairs shown here.

<i>Orbits</i>	<i>Date 1</i>	<i>Date 2</i>	<i>Baseline (m)</i>	<i>D time (years)</i>	<i>D Range (mm)</i>
E2_07496 E1_20155	Sep 26 1996	May 23 1995	15	1.35	6±3
E1_20155 E2_08999	May 23 1997	Jan 08 1995	5	1.63	10±4
E2_07496 E2_25532	Sep 26 1996	Mar 09 2000	125	3.45	20±15

**Table 2.** *Estimated Permeable Strata of Wells*

<b>Well Name</b>	<b>perforated interval (m)</b>	<b>permeable beds (m)</b>	<b>Imperm. beds (m)</b>	<b>Imperm. thickness</b>
1	86-200	84	30	26 %
2	78-202	111	13	10 %
3	81-204	105	18	14 %
San Felipe	75-170	76	20	19 %

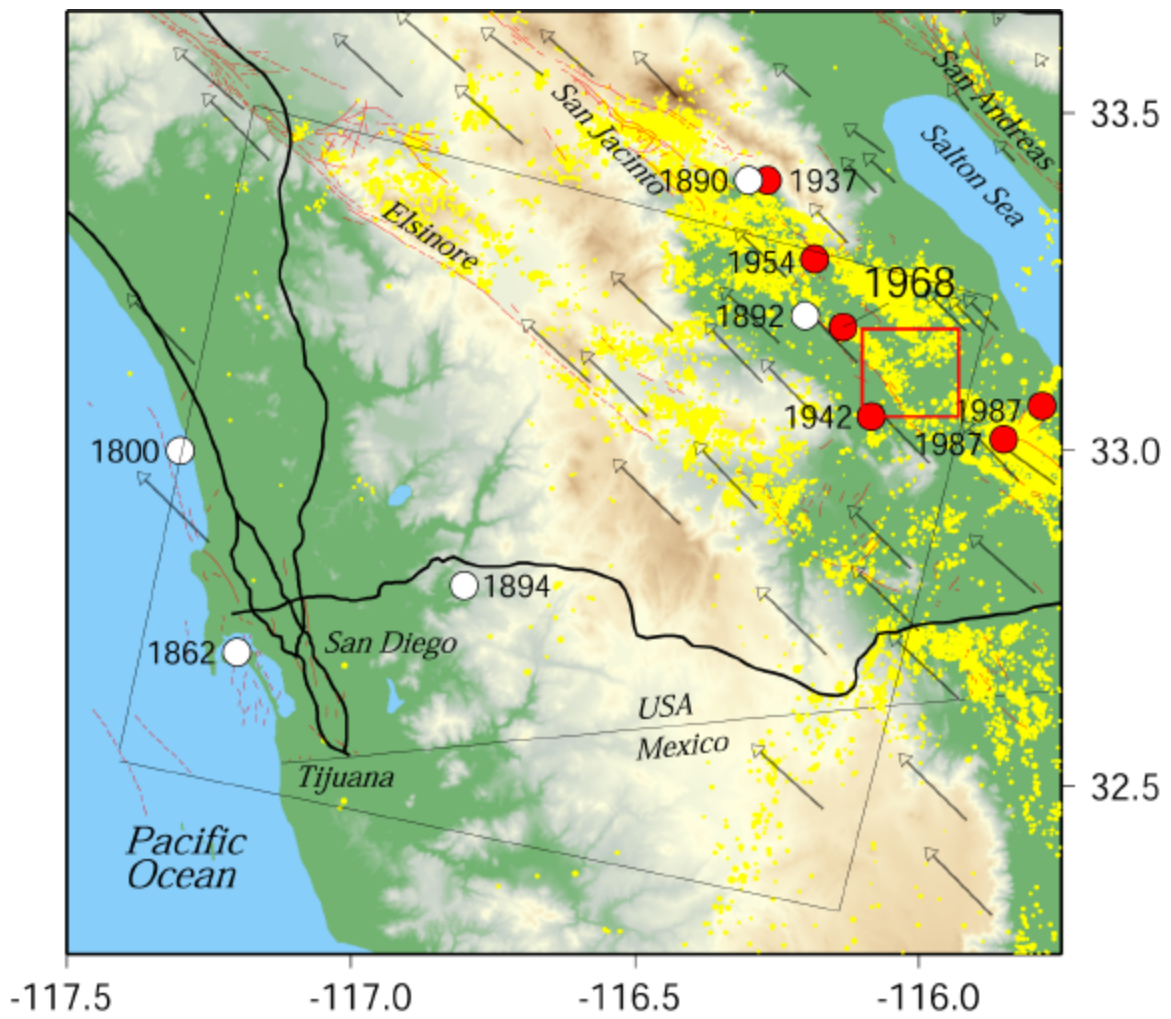


**Figure 1.**

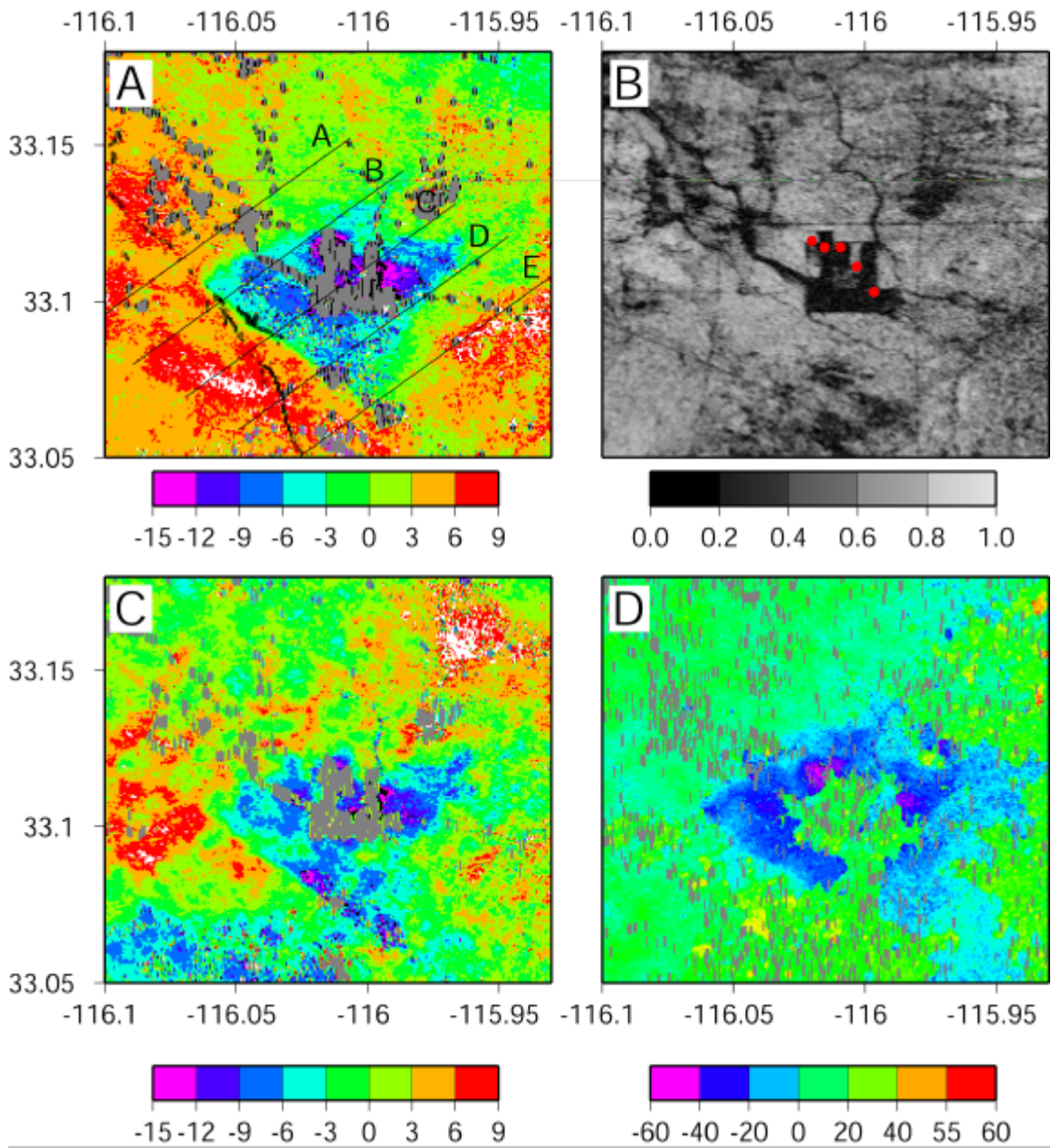


**Figure 2.**

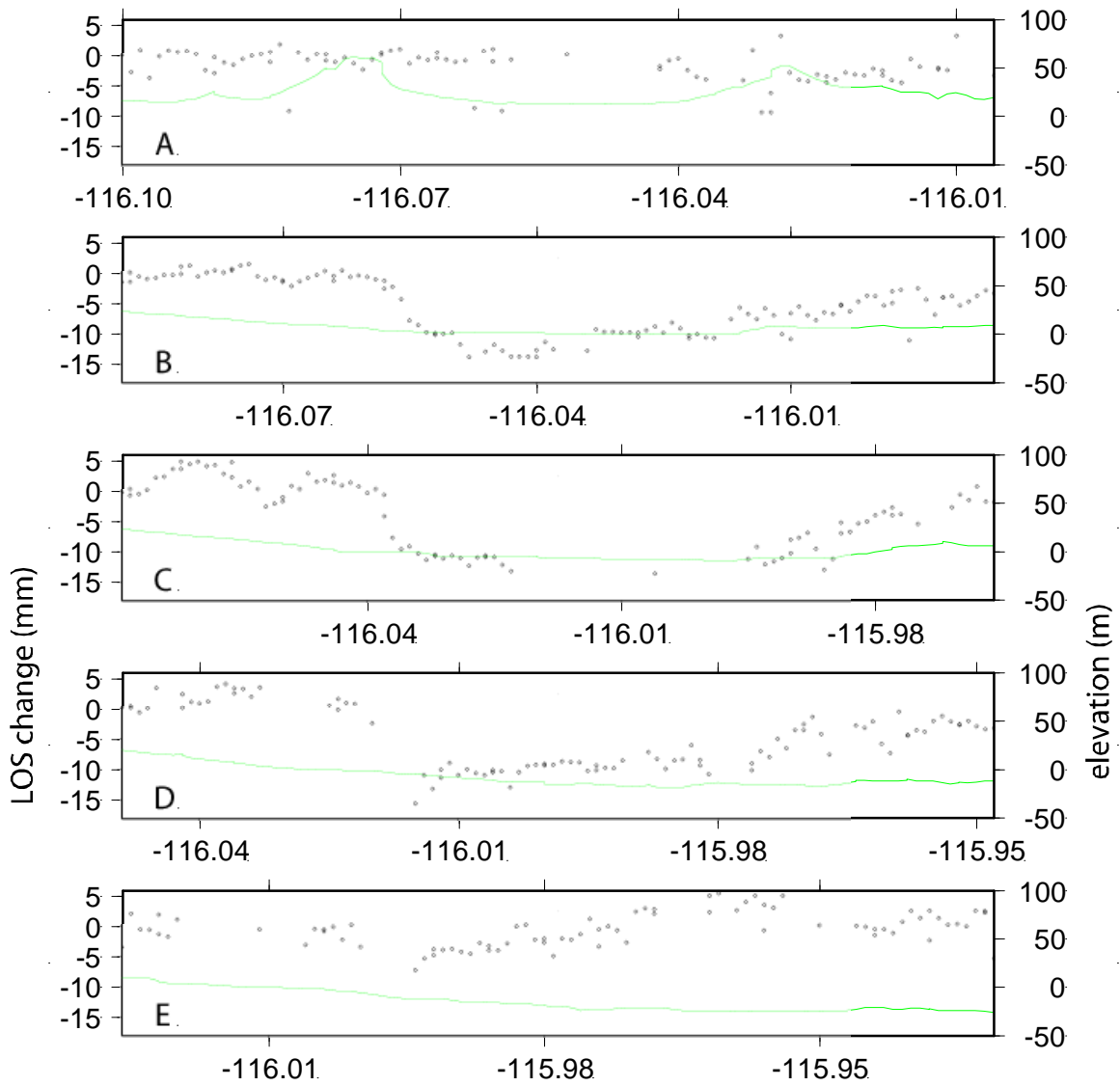
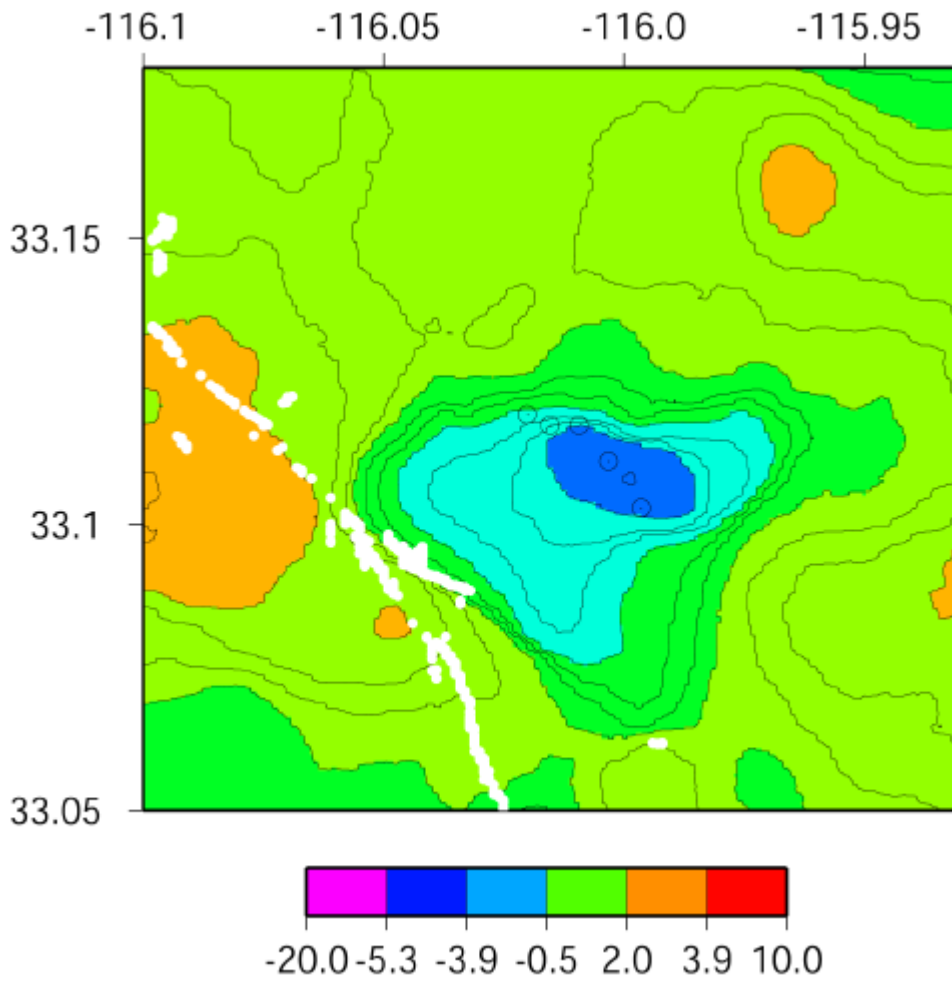


Figure 3.



**Figure 4.**

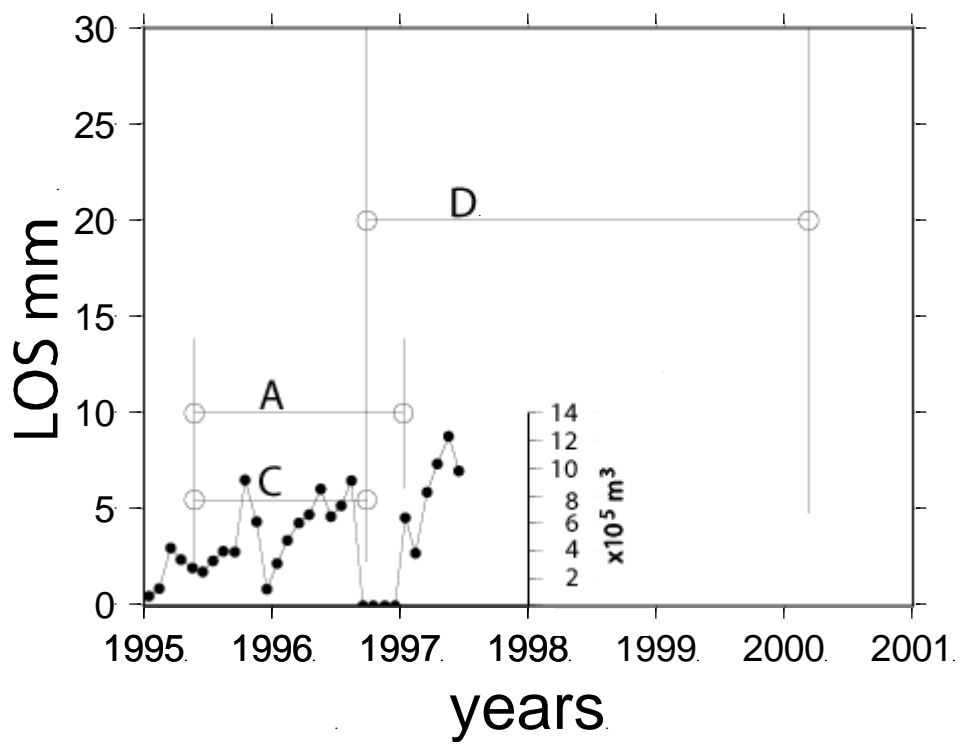
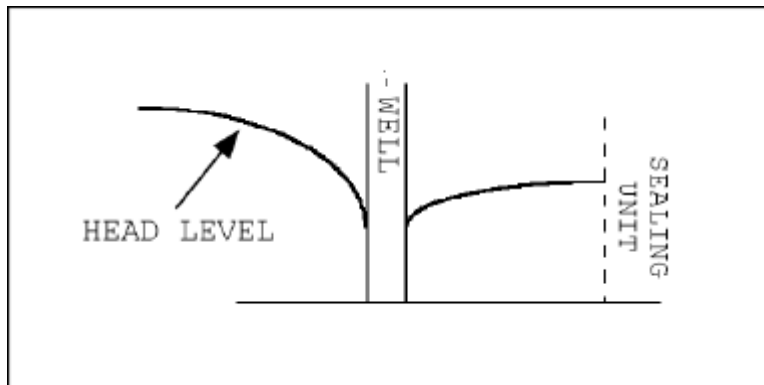


Figure 5.



**Figure 6.**